Matter and Radiation at Extremes | RESEARCH ARTICLE | scitation.org/journal/mre

Bonding-unsaturation-dependent superconductivity in P-rich sulfides

Cite as: Matter Radiat. Extremes 7, 048402 (2022); doi: 10.1063/5.0098035
Submitted: 4 May 2022 • Accepted: 15 June 2022 •
Published Online: 8 July 2022

View Online Export Citation CrossMark

Xing Li,[1] Xiaohua Zhang,[1,2] Yong Liu,[1] and Guochun Yang[1,2,a)]

AFFILIATIONS

[1] State Key Laboratory of Metastable Materials Science and Technology and Key Laboratory for Microstructural Material Physics of Hebei Province, School of Science, Yanshan University, Qinhuangdao 066004, China
[2] Centre for Advanced Optoelectronic Functional Materials Research and Key Laboratory for UV Light-Emitting Materials and Technology of Northeast Normal University, Changchun 130024, China

Note: This paper is a part of the Special Topic Collection on High Pressure Science 2022.
[a)] **Author to whom correspondence should be addressed:** yanggc468@nenu.edu.cn

ABSTRACT

The covalent frameworks found in certain compounds, such as the S–H skeleton in H_3S and the H cage in LaH_{10}, play an essential role in their superconductivity. These compounds have the feature of bonding unsaturation (a deficiency of electrons in their covalent bonding) in common. Developing an understanding of the relationship between superconductivity and bonding unsaturation in these materials can provide new ideas for the design of superconducting materials. In this work, we explored the high-pressure phase diagram of binary P–S compounds using first-principles swarm structural calculations. In addition to the previously reported P_2S and P_3S structures, we identified that P_5S, P_8S, and $P_{11}S$ also have a common structural character of six-coordinated octahedral networks; however, their bonding unsaturation are distinct due to the different valence electron numbers and unequal ratios of P and S atoms. These features provide an ideal model for exploring the bonding-unsaturation dependence of superconductivity. We estimated the average bonding unsaturation of these P-rich compounds based on the valence electron numbers and the coordination numbers of the central P/S atoms. Interestingly, the resultant average bonding unsaturation was found to be proportional to the predicted superconducting transition temperature. This finding was also verified in MH_9 (M = Y, Th, and Pr) and doped H_3S (Si, C, and P) compounds. Our work provides an opportunity to gain a deeper understanding of bonding-unsaturation-dependent superconductivity.

I. INTRODUCTION

Pressure, as an external control method, can stabilize exotic compounds that defy the traditional understandings of stoichiometry, structural form, and properties in ambient conditions.[1–4] One of the most representative cases of this phenomenon is the burgeoning field of high-pressure superconducting hydrides, which have remarkably high critical temperatures (T_c > 200 K).[5–9] Within these compounds, H atoms or H and other atoms can form rigid covalent motifs, exhibiting diverse coordination configurations such as symmetric S–H–S bonds (twofold coordination) in H_3S, 1D nanotubes via threefold coordination in HfH_9,[10] 2D penta-graphene containing twofold and threefold coordination in HfH_{10},[11] and 3D cages with fourfold coordination in LaH_{10} and CaH_6.[12–14] These coordination patterns are much beyond the bonding limit of single-electron H atoms at ambient pressure, and their corresponding covalent bonds thus possess fewer electrons than a conventional shared electron pair, appearing to be unsaturated. Strikingly, these kinds of H frameworks have been demonstrated to be able to induce strong electron–phonon coupling (EPC).[15] Thus far, the understanding of unsaturated-bonding-related superconductivity is quite limited. However, bonding unsaturation could provide a new approach to the design of superconductors.

Phosphorus (P) and sulfur (S), as adjacent elements in the Periodic Table, have moderate electronegativity as well as a strong ability to form rich P/S allotropes[16–19] and P–S compounds.[20–24] Interestingly, the majority of P–S compounds exhibit cage-like

structures,[21–24] and this bestows them with intriguing properties and gives them a broad range of potential applications.[25,26] For instance, P_4S_3, which has strong resistance to volume changes during electrochemical reactions, is considered as an ideal anode material with high capacity and cycling stability for $Li^+/Na^+/K^+$ storage, providing a reversible capacity of up to 1266 mAh g^{-1} in Li–ion batteries.[25] P_4S_{10}, having high chemical and electrochemical stability, can act as a protective layer for anodes, overcoming the corrosion and dendrite problems of Li metal anodes.[26]

In ambient conditions, P and S, which have $3s^23p^3$ and $3s^23p^4$ valence electrons, usually show three-/two-coordination in their covalent compounds, satisfying the well-known octet rules. However, in their high-pressure allotropes and compounds, their coordination numbers can be boosted to 8 and 6, respectively,[17–19,27] resulting in the formation of diverse covalent frameworks with notable bonding unsaturation, contrasting with the classical covalent bonds formed by sharing an electron pair. This unique bonding means that P and S are two significant candidate elements for high-T_c superconductors.[28–31]

The first experimental validation of a superconducting hydride ($T_c > 200$ K) was conducted with H_3S, which has a record T_c of 203 K at 155 GPa,[32] and this consists of nested SH_6 octahedral networks with each other.[4] Moreover, monoclinic ($C2/m$) PH_3, with a P–H covalent framework and six-coordinated P, exhibits a maximum T_c of 83 K at 200 GPa in P-H compounds.[30] Based on the difference in valence electrons, the S atoms in H_3S can be partially substituted with non-metallic atoms from the IV-, V-, VI-, or VII-A groups,[33–36] and this can be used to modulate the position of the van Hoff singularity with respect to the Fermi level (E_F), raising the T_c value. In fact, the bonding unsaturation in doped H_3S can also be tuned. Interestingly, the T_c value has been found to increase significantly to 290 K at 250 GPa after replacing 7.5% of the S atoms with P atoms.[34] To date, numerous binary and ternary P- and S-based compounds have been predicted to exhibit excellent superconductivity associated with their various covalent networks.[37–41]

Pressure-induced P–S compounds have also attracted great research interest due to the unique bonding behavior of P and S atoms. In particular, two pioneering works explored the exotic properties of P–S compounds at high pressure.[42,43] Li *et al.* found that as the pressure increases, the stable phases (e.g., P_2S_7 and P_4S_x, $x = 3$–10) at 0 GPa gradually decompose, and above 8 GPa, the only predicted stable phase is R-3m PS_2; this was confirmed by experiments.[42] More interestingly, R-3m PS_2, which is isostructural to 3R MoS_2, is a van der Waals layered compound with a predicted T_c of ~11 K at 0 GPa. In addition, Liu *et al.* found several P–S compounds including P_3S, P_2S, PS, PS_2, and PS_3, showing abundant S- and P-centered polyhedrons (e.g., SP_6, SP_4, SP_3, PS_6, and PS_3).[43] However, there is a difference regarding the stability of high-pressure PS_2 phases: $C2/m$ and P-3m1 PS_2 were found to stable from 5 to 200 GPa in Liu *et al.*'s work,[43] but the synthesized R-3m phase disappears.[42] In summary, the veil over the nature and behavior of P–S compounds at high pressure has not yet been fully lifted.

Taking into account the peculiar bonding behavior of P and S atoms and the imperfect high-pressure P–S phase diagram, herein, we perform a comprehensive structural search with various stoichiometries P_xS_y ($x/x + y = 0$–1, 38 compositions) to explore as-yet untapped P–S compounds and their electronic properties. Three unknown P-rich phases, $Cmcm$ P_5S, P-31m P_8S, and P-1 $P_{11}S$, were identified, in which both P and S atoms present sixfold octahedral coordination with unsaturated covalent bonds, inducing superconductivity. Furthermore, in P-rich P–S compounds and several MH_9 hydrides, a positive correlation was established between unsaturated bonding and the superconducting transition temperature, indicating the feasibility of modulating bonding saturation to improve superconductivity. In addition to the three proposed PS_2 phases, a new low-pressure P-3m1 PS_2 phase was found, representing a missing link in the phase-transition sequence with increasing pressure.

II. COMPUTATIONAL DETAILS

An intelligence-based particle swarm optimization algorithm using the CALYPSO software package has been demonstrated to be an important way to discover new structures.[7] In this work, structures with various P_xS_y compositions ($x = 1$, $y = 1/12$, 1/11-1/3, 3/8, 2/5, 1/2, 3/5, 2/3, 3/4, 4/5, 1, 5/4, 4/3, 3/2, 5/3, 7/4, 2, 9/4, 5/2, 8/3, 3, 7/2, 4, 5-12) were extensively searched with simulation cell sizes of 1–4 formula units at 25, 50, 100, and 200 GPa. Structural relaxation and electronic structure calculations were carried out within framework of density functional theory with the Perdew–Burke–Ernzerhof generalized gradient approximation,[44] as implemented in the Vienna *Ab initio* Simulation Package.[45] Projector augmented waves with $3s^23p^3$ and $3s^23p^4$ electrons were used as valences for P and S atoms, respectively.[46] The reliability of our adopted pseudopotentials was confirmed by the perfect fitting of the Birch–Murnaghan equation of states with the full-potential linearized augmented-plane-wave method [Fig. S3(a)]. A plane-wave cutoff energy of 600 eV and a Monkhorst–Pack scheme with a k-point grid of $2\pi \times 0.03$ Å^{-1} in the Brillouin zone were used to ensure an enthalpy convergence of less than 1 meV/atom. The electron localization function (ELF) is used to describe and visualize the chemical bonds of the stable compounds.[47] The integrated crystal orbital Hamilton population (ICOHP) was calculated using the LOBSTER software package.[48] Phonon-dispersion curves were calculated using the supercell finite-displacement method in the Phonopy software package.[49]

The EPC calculations were carried out within the framework of density-functional perturbation theory, as executed in the Quantum ESPRESSO package.[50] We employed ultrasoft pseudopotentials, with $3s^23p^3$ and $3s^23p^4$ considered as the valence electrons for P and S, respectively. A kinetic-energy cutoff of 70 Ry and Gaussians of width 0.02 Ry were applied. To reliably calculate the EPC in metallic systems, we need to sample dense k-meshes for the electronic Brillouin zone integration and enough q-meshes to evaluate the average contributions from the phonon modes. Dependent on specific structures of the stable compounds, different sizes of k- and q-meshes were used: $15 \times 15 \times 9$ k-meshes and $5 \times 5 \times 3$ q-meshes for P_2S in the $C2/m$-I structure, $12 \times 12 \times 3$ k-meshes and $3 \times 3 \times 3$ q-meshes for P_3S in the $C2/m$ structure, $15 \times 15 \times 6$ k-meshes and $5 \times 5 \times 2$ q-meshes for P_5S in the $Cmcm$ structure, $8 \times 8 \times 12$ k-meshes and $4 \times 4 \times 6$ q-meshes for P_8S in the P-31m structure, and $12 \times 12 \times 9$ k-meshes and $4 \times 4 \times 3$ q-meshes for $P_{11}S$ in the P-1 structure.

III. RESULTS AND DISCUSSION

To explore the phase diagram of the P–S system, an extensive structure search was performed by focusing on the 38

stoichiometries. The relative stabilities of the P_xS_y compounds were determined using their formation enthalpies with respect to the solid phases of P[27] and S[18,51] at the considered pressures (Fig. S1). We not only reproduced the theoretically proposed[42,43] $C2/m$ P_3S, $C2/m$-I P_2S, $C2/m$-II P_2S, $P2_1/m$ PS, R-3m PS_2, $C2/m$ PS_2, P-3m1 PS_2, and $C2/c$ PS_3 structures at high pressures, but also identified three hitherto unknown P-rich compounds: $Cmcm$ P_5S, P-31m P_8S, and P-1 $P_{11}S$ [Fig. 1(a)], as well as a new P-3m1 PS_2 phase (labeled as P-3m1-I, Fig. S2).

The optimized lattice parameters of R-3m PS_2 (a = 3.165 Å and c = 15.572 Å) were found to be in good agreement with the experimentally obtained values (a = 3.149 Å, and c = 15.501 Å) at 14 GPa;[42] additionally, the use of different exchange–correlation functionals did not affect the thermodynamic stabilities of the phases proposed here [Fig. S3(b)], confirming the reliability of our calculations. Both

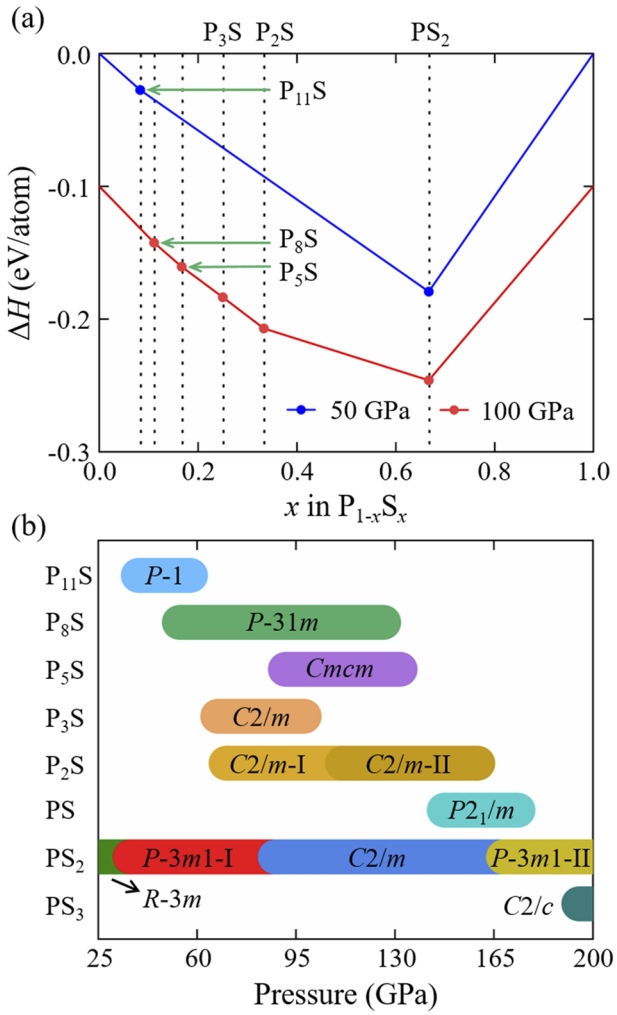

FIG. 1. (a) Convex hull constructed with thermodynamically stable P–S compounds at 50 and 100 GPa. For clarity, we have offset the formation enthalpy by −0.1 eV for 100 GPa. The full convex hull is shown in Fig. S1. (b) Pressure–composition phase diagram of stable P–S compounds.

$C2/m$ and $C2/c$ PS_3 were predicted by Liu *et al.* to be thermodynamically stable.[43] However, in our work, we found that only the $C2/c$ phase is thermodynamically stable. In other words, $C2/m$ PS_3 is unstable against decomposition into S and PS_2 in our considered pressure range of 25–200 GPa, as shown in Fig. S2(b). All the predicted structures are dynamically stable due to the absence of any imaginary frequencies in the phonon dispersion curves (Fig. S4). The stabilizing pressure ranges of the identified phases are illustrated in Fig. 1(b), and this provides useful information for experiments.

There are obvious differences in the stable stoichiometries and structural characters between high and ambient pressures. Most of the P–S compounds are S-rich stoichiometries with the structural features of a cage-like molecular crystal in P_4S_x (x = 5, 7, 9, and 10) and infinite wrinkled chains in P_2S_7 at ambient pressure.[20–24] Increasing the S content in the compounds induces a gradual transformation of coordination configuration from triangular cone to tetrahedron for the P atoms, and this is accompanied by an increase of the coordination number (Fig. S5). In sharp contrast, at high pressure, P-rich stoichiometries are stabilized (P_xS, x = 5, 8, and 11). Notably, these P-rich compounds exhibit similar P–S frameworks, including the reported P_2S and P_3S, which can be viewed as derivatives of S-doped simple cubic (sc) P [Figs. 2(a)–2(c)]. In other words, both the P and S atoms in these structures maintain a six-coordinated octahedron configuration independent of the P/S ratio, but the S-centered octahedra demonstrate different coordination atoms, such as four P atoms and two S atoms in P_2S, or mixed four P and two S atoms as well as six P atoms in P_3S, as well as six P atoms in P_xS (x = 5, 8, and 11) at 100 GPa (Fig. S6).

The P/S ratio can be used to effectively modulate the orientation and distribution of S-centered octahedra. Specifically, in P_2S, P_3S, and $P_{11}S$, S-centered octahedra are distributed horizontally with S atoms in the same layer, leading to the formation of alternating P layers perpendicular to the horizontal plane [Figs. S6(a), S6(b), and S6(f)]. In P_5S and P_8S, the central S atoms are alternately distributed in different directions, inhibiting the formation of the P layer [Figs. S6(c)–S6(e)]. As a result, different connections appear between the S-centered octahedra, including mixed edge/vertex sharing in P_2S and P_3S, vertex sharing in P_5S, and P_2 pair sharing in P_8S and $P_{11}S$. In the P_xS (x = 5, 8, and 11) compounds, the P–P and P–S bond lengths are in the range 2.12–2.17 Å at 100 GPa, which is close to the P–P (2.20 Å) and P–S (2.09 Å) bond lengths in black phosphorus and P_4S_3 at ambient pressure,[52,53] indicating that covalent P–P/S bonds are responsible for the stabilization, as demonstrated by the ELF [Fig. 4(a) and Fig. S7].

As noted in the introduction to this paper, the previously reported stable phases of PS_2 are discrepant under pressure. Aside from the R-3m phase being stable in the range 8–20 GPa,[42] the $C2/m$ and P-3m1 phases are found to be stable in the ranges 5–178 and 178–200 GPa,[43] respectively. Here, we not only reproduce the stable R-3m, $C2/m$, and P-3m1 phases, but we also identify a new P-3m1-I phase, which stabilizes from 36.3 to 87.6 GPa; this is an intermediate phase between the R-3m and $C2/m$ phases. Notably, the discovery of the P-3m1-I phase settles the contradiction regarding the PS_2 phase diagram and provides a plausible description of the phase-transition process of PS_2 with pressure.

For R-3m PS_2 with an ABC stacking order, pressure makes the sublayers slide along ab plane into AA stacking, accompanying the transition from the R-3m phase to the P-3m1-I phase (Fig. S8). With

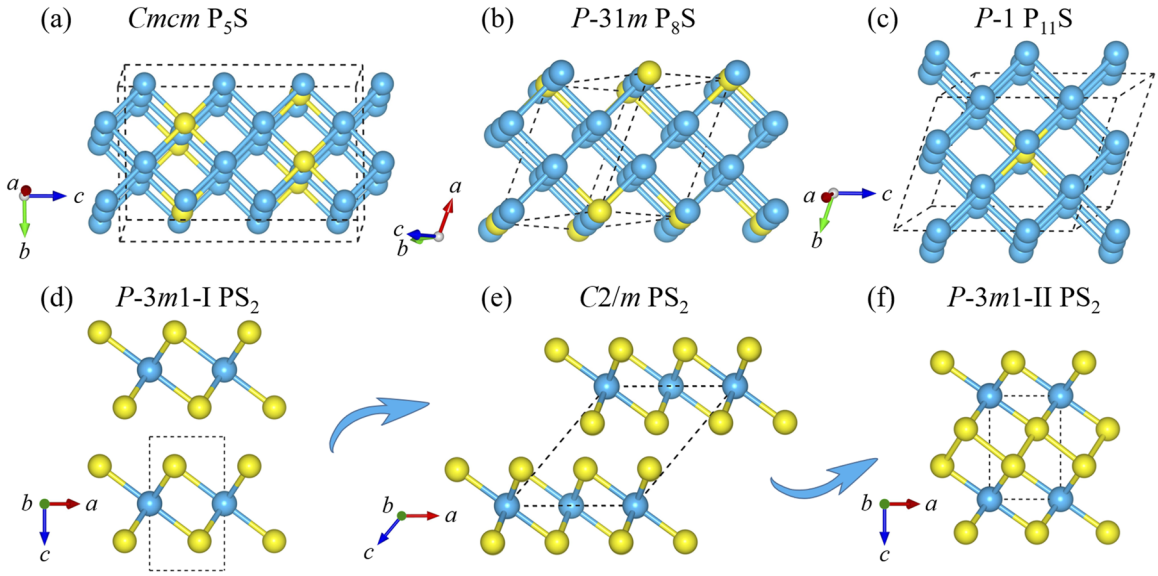

FIG. 2. Crystal structures of (a) *Cmcm* P_5S at 100 GPa, (b) *P*-31*m* P_8S at 100 GPa, (c) *P*-1 $P_{11}S$ at 50 GPa, (d) *P*-3*m*1-I PS_2 at 50 GPa, (e) *C*2/*m* PS_2 at 100 GPa, and (d) *P*-3*m*1-II PS_2 at 200 GPa. Blue and yellow spheres represent P and S atoms, respectively.

further compression, the sublayers in the *P*-3*m*1-I phase move away from each other along the *a* axis until transitioning into *C*2/*m* symmetry with staggered sublayers in the vertical direction [Figs. 2(d) and 2(e)]. Then, the PS_2 sublayers in the *C*2/*m* phase move toward each other along the *a* axis with increasing pressure. Finally, AA stacking *P*-3*m*1-II PS_2 is obtained above 168.3 GPa [Figs. 2(e) and 2(f)], in which both S and P atoms form a covalent octahedron coordination (e.g., S-centered P_3S_3 and PS_6). Overall, the lattice parameters and distances between S atoms of adjacent sublayers progressively decrease with pressure (Fig. S9). Meanwhile, the charge is redistributed and the interlayered S–S interaction is enhanced, as supported by the ELF (Fig. S10), resulting in a transformation of PS_2 from a van der Waals layered structure to a 3D covalent framework.

One prominent structural characteristic is the formation of covalent octahedron coordination for P and S atoms in P-rich P–S compounds at high pressure. This is mainly attributed to the head-to-head overlap of three p-orbital wave functions [Fig. 3(a)], as verified below. Here, we follow the principle from simplicity to complexity. First, sc P is selected due to the identical orthometric basis vector between the crystal structure and the covalent bond orientation. The calculated ICOHP exhibits dominant bonding interactions between the p_x and p_x, p_y and p_y, and p_z and p_z orbitals along the three bonding directions (Fig. S11). Meanwhile, P 3s electrons are involved in bonding with the 3p electrons of corresponding orientation. A similar bonding pattern is also demonstrated in *Im*-3*m* H_3S (Fig. S12). Similarly, P_xS compounds follow the bonding pattern of P_8S (Figs. S13 and S14) by excluding the basis-vector difference between the atomic p orbitals and the covalent bond orientations.

The corresponding covalent bonds for P atoms in these P-rich compounds have unsaturated bonding due to there being five valence electrons from each P atom for six bonds. Here, we propose a standard for evaluating the unsaturation of covalent bonds in these compounds. Each S or P atom has 6 or 5 valence electrons, respectively. On average, a single S atom can provide one electron per covalent bond in a six-coordinated octahedron, whereas a P atom can provide 5/6 of an electron. Therefore, the number of electrons is $(1 + 1)e^-$ in each S–S bond, $(1 + 5/6)e^-$ in each P–S bond, and $(5/6 + 5/6)e^-$ in each P–P bond; the S–S bonds are saturated (e.g., a two-centered two-electron bond), and the other two are unsaturated.

For ease of measuring the covalent unsaturation of these three kinds of bonds, the saturation of each S–S bond is normalized to 1—meaning that the saturations of P–S and P–P bonds are 0.917 and 0.833, respectively—and the bonding unsaturation is defined to be the difference between 1 and the saturation, e.g., 0, 0.083, and 0.167 for S–S, P–S, and P–P bonds, respectively. Correspondingly, the average bonding unsaturation of these five P-rich P–S compounds is 0.106 for P_2S, 0.125 for P_3S, 0.139 for P_5S, 0.148 for P_8S, and 0.153 for $P_{11}S$ [Fig. 3(b)], the detailed calculations can be found in supplementary material. It is apparent that the average bonding unsaturation increases monotonously with increasing P content.

The calculated projected densities of states (PDOS) illustrate that P_5S, P_8S, and $P_{11}S$ are metallic on account of the large electronic contributions at E_F [Fig. 4(b) and Fig. S15]. The considerable orbital overlap between P and S atoms (3p–3p, and 3s–3s) also supports their strong covalent interaction. With respect to P/S 3s states, the 3p states have a much larger DOS at E_F, dominating the metallicity of these P–S compounds. Notably, their DOS amplitude at E_F (N_{E_F}) is consistent with the average bonding unsaturation. i.e., the larger the average bonding unsaturation, the higher the PDOS amplitude [Fig. 3(d)].

On account of the identical coordination modes and distinct bonding unsaturation values caused by different P/S ratios in

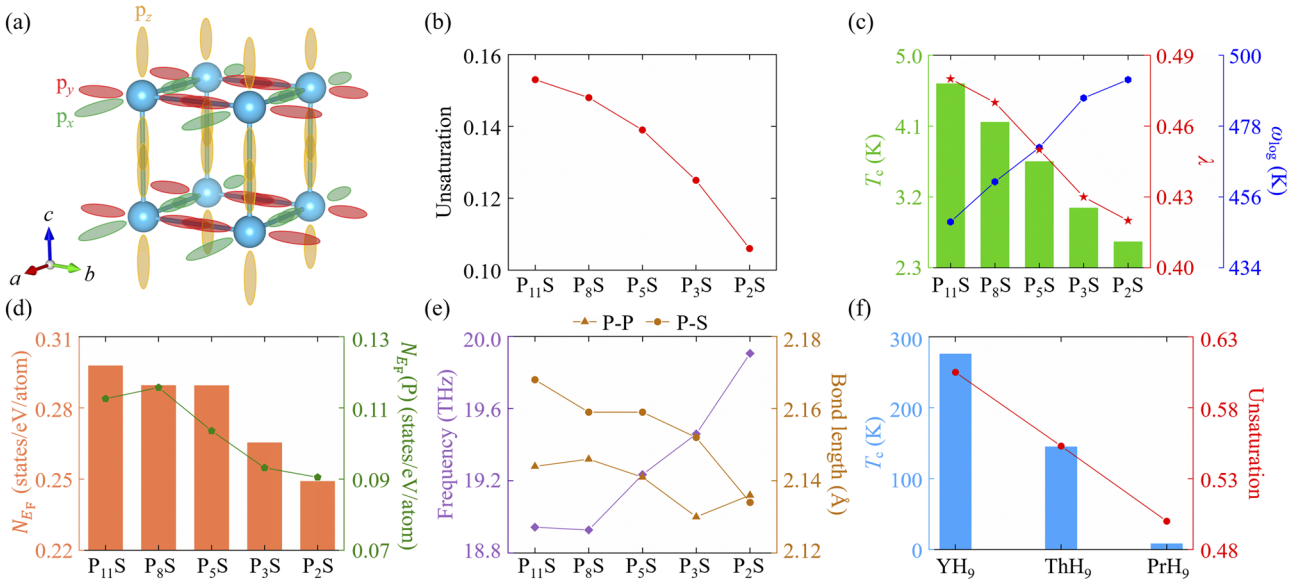

FIG. 3. (a) Schematic diagram of the bonding mechanism in sc P. (b) Average bonding unsaturation, (c) T_c and EPC parameters λ, and the logarithmic average phonon frequency ω_{log} values, (d) total DOS N_{E_F} per atom, and PDOS of P atom N_{E_F}(P) at E_F, (e) lengths of P–P and P–S bonds, and the highest phonon frequency of five P-rich P–S compounds (P_2S, P_3S, P_5S, P_8S, and $P_{11}S$). (f) T_c and calculated average bonding unsaturation values of H_{29} cage assuming that all valence electrons of the transition metal (TM) are transferred to the H cages in well-known superconducting TM hydrides ($P6_3/mmc$ TMH_9, TM = Y, Th, and Pr) at 120–150 GPa.

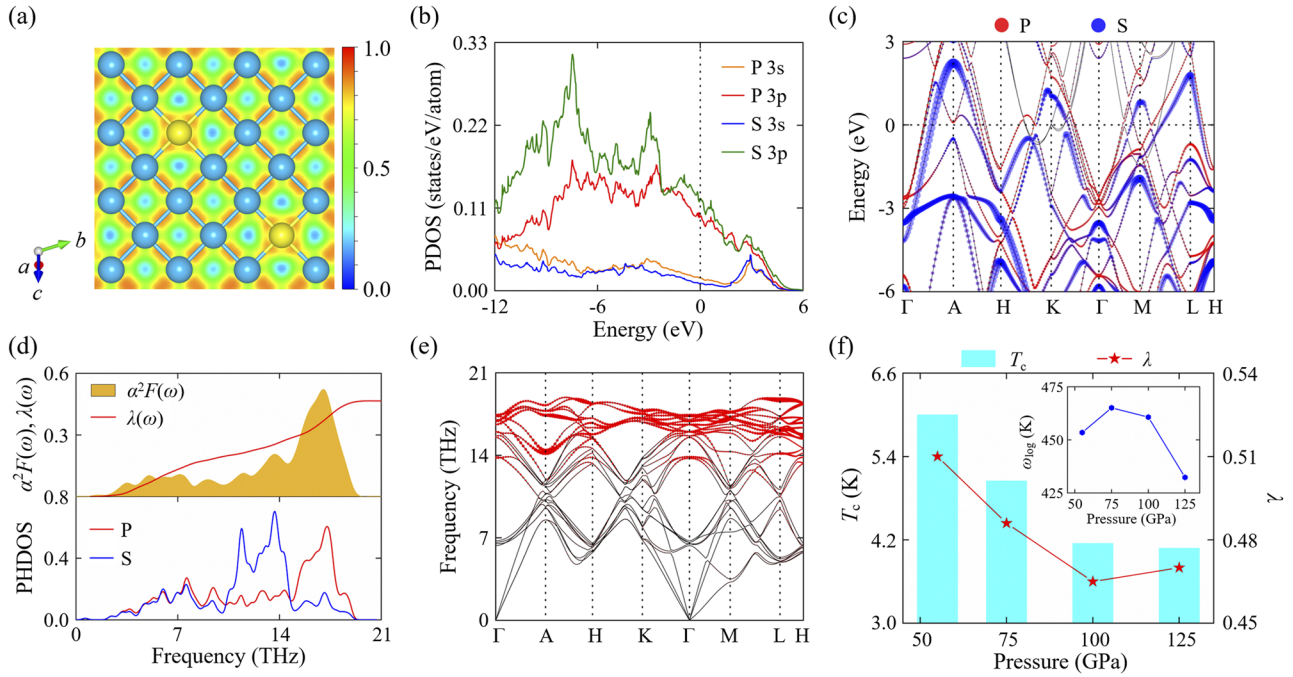

FIG. 4. (a) ELF, (b) PDOS, (c) projected electronic band structure, (d) PHDOS and Eliashberg spectral function and $\lambda(\omega)$, (e) phonon dispersion curves (the magnitude of λ is indicated by the thicknesses of the red curves), and (f) pressure-dependent T_c, λ, and ω_{log} of P-31m P_8S.

P-rich compounds (e.g., P_2S, P_3S, P_5S, P_8S, and $P_{11}S$), they provide an ideal model for the study of bonding-unsaturation-related superconductivity. To accurately describe this relationship, we calculated their T_c values at an identical pressure (e.g., 100 GPa) by employing the Allen–Dynes-modified McMillan equation.[54] Here, the T_c values of the previously proposed $C2/m$-I P_2S and $C2/m$ P_3S structures are recalculated for better comparability. The resulting T_c values (2.63 K for $C2/m$-I P_2S, 3.06 K for $C2/m$ P_3S) are in accordance with the reported values (Fig. S17).[43] Interestingly, the value of T_c increases monotonously with the increasing average bonding unsaturation from P_2S to $P_{11}S$, indicating an evident positive correlation between bonding unsaturation and T_c values [Fig. 3(c)]. Furthermore, their λ values present the same evolution trend with T_c values; the trend in ω_{log} is opposite, manifesting a decisive effect of λ on the variation of T_c value.

The increasing λ value can be principally ascribed to the elevated N_{E_F} value, especially for P-derived DOS contributions at E_F [Fig. 3(d)]. This is related to the increase of the number of P–P bonds, which have greater bonding unsaturation than P–S bonds. However, the variation of the highest phonon frequency of P_xS compounds is inverse to the average bonding unsaturation, which may be derived from the lengthening of P–S and P–P bonds [Fig. 3(e)]. The lowering of the phonon frequency leads to a reduction in ω_{log}. However, the decreasing phonon frequency ω is also favorable to raising λ according to its definition formula $\lambda = 2\int d\omega \frac{\alpha^2 F(\omega)}{\omega}$.[55,56] Overall, a higher bonding unsaturation favors the superconductivity of P_xS compounds.

To further examine the effect of bonding unsaturation on superconductivity, we inspected reported superconducting TM hydrides based on these criteria: they must have the same H cage, different electrons donated by TM atoms that affect bonding saturation, and pressure differences within 30 GPa to minimize the effects of pressure. Among the three well-known TMH_x clathrates (LaH_{10}-type with H_{32} cage, YH_9-type with H_{29} cage, and CaH_6-type with H_{24} cage),[57] only YH_9-type clathrates can meet these requirements. Here, we assume that the smaller the number of TM valence electrons, the higher the average bonding unsaturation of the H cage. This is also confirmed by the calculated charge-transfer amount (Fig. S16).

As shown in Fig. 3(f) and Fig. S16, with increasing average bonding unsaturation, the T_c values of TMH_9 (M = Y, Th, and Pr) present an increasing trend.[57–59] This is also similar to the T_c evolution of H_3S after incorporating a small number of Si/C/P atoms, i.e., doped H_3S with more electron-deficient atoms than the S atom can elevate the bonding unsaturation and the corresponding T_c values (e.g., T_c = 283 K at 230 GPa, 220 K at 225 GPa, and 212 K at 200 GPa for 4% Si, 7% C, and 6.25% P-doped H_3S with average bonding unsaturations of 0.257, 0.262, and 0.255, respectively, higher than H_3S).[33,60,61] These results provide further support for the relationship between bonding unsaturation and superconductivity. It is noteworthy that our work opens the door to greater understanding of bonding-unsaturation-dependent superconductivity; further efforts are needed for a deeper understanding.

To explore the origin of superconductivity in these materials, we take P_8S as an example due to it having the highest structural symmetry and the widest stabilizing pressure range among the P-rich compounds. The projected electronic band structure of P_8S reveals obvious P–S hybridization across the whole Brillouin zone [Fig. 4(c)]. Moreover, several bands crossing E_F demonstrates steep dispersion along the Γ–A, A–H, and L–H directions, as well as a flat feature around the K point [Fig. 4(c)]. The calculated EPC parameter (λ) of P_8S is 0.47 at 100 GPa [Fig. 4(d)], and this is comparable to the values of 0.52 for $C2/m$ S_3PH at 150 GPa,[37] 0.59 for $Cmcm$ PH_3 at 100 GPa,[31] and 0.42 for $Pnma$ H_4S_3 at 140 GPa,[62] and it is slightly lower than the value of 0.64 for $Cmc2_1$ SP_2H at 150 GPa.[37] Based on the Eliashberg spectral function $\alpha^2F(\omega)$ and the phonon density of states (PHDOS), we can establish that the phonons derived from P and S atoms show evident coupling across the whole phonon frequency range due to their similar mass and strong covalent interactions; the phonons in the frequency range 10.0–18.9 THz make the main contribution (59%) to the total λ, and these correspond to two large S- and P-dominated PHDOS peaks [Fig. 4(d)]. In particular, above 14.5 THz, there appears to be a rapid increase in λ, resulting in a large contribution of 40%; this is also illustrated in the phonon dispersion curves [Fig. 4(e)]. Such a strong EPC is thus mainly associated with P-atom vibrations and local phonon softening at the A point. Based on the Allen–Dynes-modified McMillan equation,[54] the T_c value of P_8S is estimated to be 4.15 K at 100 GPa with a typical Coulomb pseudopotential parameter of $\mu^* = 0.1$.[63,64] Combining this with the electronic band structure, we can draw the conclusion that the superconductivity of P_8S principally comes from the coupling between the P/S 3p electrons and the P-/S-derived phonons.

To obtain insight into the pressure dependence of the superconductivity of P_8S, we investigated its superconductivity in the pressure range 55–125 GPa. The variation of T_c and the two key parameters (λ and ω_{log}) with pressure are displayed in Fig. 4(f). As the pressure decreases, T_c gradually increases, reaching a maximum of 6.0 K at 55 GPa. Below 100 GPa, the variation of λ is linearly related to T_c; this is in sharp contrast to ω_{log}, indicating that λ dominates the evolution of T_c. Above 100 GPa, the value of λ increases slightly, whereas ω_{log} decreases significantly, and this is responsible for the evolution of T_c. Overall, the pressure dependence of T_c is the result of competition between λ and ω_{log}.

IV. CONCLUSIONS

In summary, we performed an extensive first-principles structural search of P–S systems under high pressure and identified three stable P-rich compounds ($Cmcm$ P_5S, P-31m P_8S, and P-1 $P_{11}S$) and a new low-pressure PS_2 phase with P-3m1 symmetry, which acts as an intermediate phase between the R-3m and $C2/m$ phases, completing the understanding of the phase-transition process of PS_2. All the P-rich P_xS ($x > 1$) compounds have a common covalent framework, in which P and S atoms form an octahedral coordination via head-to-head hybridization of P/S 3p orbitals and unsaturated covalent bonds. More interestingly, the variation in bonding unsaturation induced by different P contents is nearly linearly related to the N_{E_F} value, the EPC parameter λ, and the T_c value. A similar relationship is also observed in MH_9-type clathrates and Si/C/P-doped H_3S. Furthermore, the superconducting origin of this kind of compound is closely associated with the coupling of 3p electrons with the middle-/high-frequency phonons of P/S atoms. Our results indicate that modulating the bonding unsaturation in covalent frameworks could be a useful strategy for improving superconductivity.

SUPPLEMENTARY MATERIAL

See supplementary material for full computational details, tests of the adopted pseudopotentials, phase stability, crystal structures, ELF, PDOS, PHDOS, Eliashberg spectral function, EPC parameters, structural information of P-rich sulfides, ELF, pressure-dependent lattice parameters and S–S distances between adjacent sublayers of the stable PS_2 phases, the structural units of P–S compounds at ambient pressure, ICOHP values and corresponding covalent bonds in simple cubic P, H_3S, and P_8S, the calculation of average bonding unsaturation, and a comparison of the valence electrons of TM atoms, Hirshfeld charges, and the average bonding unsaturation of the H_{29} cage in YH_9, ThH_9, and PrH_9.

ACKNOWLEDGMENTS

The authors acknowledge funding from the Natural Science Foundation of China (Grant Nos. 21873017 and 21573037), the Natural Science Foundation of Hebei Province (Grant Nos. A2019203507 and B2021203030), the Postdoctoral Science Foundation of China (Grant No. 2013M541283), and the Natural Science Foundation of Jilin Province (Grant No. 20190201231JC). This work was carried out at the National Supercomputer Center in Tianjin, and the calculations were performed on TianHe-1 (A).

AUTHOR DECLARATIONS

Conflict of Interest

The authors have no conflicts to disclose.

Author Contributions

Xing Li: Visualization (equal); Writing – original draft (equal). **Xiaohua Zhang:** Visualization (equal); Writing – original draft (equal). **Yong Liu:** Writing – review & editing (supporting). **Guochun Yang:** Resources (lead); Supervision (lead); Writing – review & editing (lead)

DATA AVAILABILITY

The data that support the findings of this study are available from the corresponding author upon reasonable request.

REFERENCES

[1]W. Lu, S. Liu, G. Liu, K. Hao, M. Zhou, P. Gao, H. Wang, J. Lv, H. Gou, and G. Yang, "Disproportionation of SO_2 at high pressure and temperature," Phys. Rev. Lett. **128**, 106001 (2022).

[2]Y. Liu, R. Wang, Z. Wang, D. Li, and T. Cui, "Formation of twelve-fold iodine coordination at high pressure," Nat. Commun. **13**, 412 (2022).

[3]Y. Chen, X. Feng, J. Chen, X. Cai, B. Sun, H. Wang, H. Du, S. A. T. Redfern, Y. Xie, and H. Liu, "Ultrahigh-pressure induced decomposition of silicon disulfide into silicon-sulfur compounds with high coordination numbers," Phys. Rev. B **99**, 184106 (2019).

[4]D. Duan, Y. Liu, F. Tian, D. Li, X. Huang, Z. Zhao, H. Yu, B. Liu, W. Tian, and T. Cui, "Pressure-induced metallization of dense $(H_2S)_2H_2$ with high-T_c superconductivity," Sci. Rep. **4**, 6968 (2014).

[5]A. R. Oganov, C. J. Pickard, Q. Zhu, and R. J. Needs, "Structure prediction drives materials discovery," Nat. Rev. Mater. **4**, 331–348 (2019).

[6]C. J. Pickard, I. Errea, and M. I. Eremets, "Superconducting hydrides under pressure," Annu. Rev. Condens. Matter Phys. **11**, 57–76 (2020).

[7]L. Zhang, Y. Wang, J. Lv, and Y. Ma, "Materials discovery at high pressures," Nat. Rev. Mater. **2**, 17005 (2017).

[8]D. V. Semenok, I. A. Troyan, A. G. Ivanova, A. G. Kvashnin, I. A. Kruglov, M. Hanfland, A. V. Sadakov, O. A. Sobolevskiy, K. S. Pervakov, and I. S. Lyubutin, "Superconductivity at 253 K in lanthanum-yttrium ternary hydrides," Mater. Today **48**, 18–28 (2021).

[9]X. Zhang, Y. Zhao, and G. Yang, "Superconducting ternary hydrides under high pressure," Wiley Interdiscip. Rev.: Comput. Mol. Sci **12**, e1582 (2022).

[10]K. Gao, W. Cui, J. Chen, Q. Wang, J. Hao, J. Shi, C. Liu, S. Botti, M. A. L. Marques, and Y. Li, "Superconducting hydrogen tubes in hafnium hydrides at high pressure," Phys. Rev. B **104**, 214511 (2021).

[11]H. Xie, Y. Yao, X. Feng, D. Duan, H. Song, Z. Zhang, S. Jiang, S. A. T. Redfern, V. Z. Kresin, C. J. Pickard, and T. Cui, "Hydrogen pentagraphenelike structure stabilized by hafnium: A high-temperature conventional superconductor," Phys. Rev. Lett. **125**, 217001 (2020).

[12]H. Liu, I. I. Naumov, R. Hoffmann, N. W. Ashcroft, and R. J. Hemley, "Potential high-T_c superconducting lanthanum and yttrium hydrides at high pressure," Proc. Natl. Acad. Sci. U. S. A. **114**, 6990 (2017).

[13]M. Somayazulu, M. Ahart, A. K. Mishra, Z. M. Geballe, M. Baldini, Y. Meng, V. V. Struzhkin, and R. J. Hemley, "Evidence for superconductivity above 260 K in lanthanum superhydride at megabar pressures," Phys. Rev. Lett. **122**, 027001 (2019).

[14]H. Wang, J. S. Tse, K. Tanaka, T. Iitaka, and Y. Ma, "Superconductive sodalite-like clathrate calcium hydride at high pressures," Proc. Natl. Acad. Sci. U. S. A. **109**, 6463 (2012).

[15]H. M. James and A. S. Coolidge, "The ground state of the hydrogen molecule," J. Chem. Phys. **1**, 825–835 (1933).

[16]F. Bachhuber, J. von Appen, R. Dronskowski, P. Schmidt, T. Nilges, A. Pfitzner, and R. Weihrich, "The extended stability range of phosphorus allotropes," Angew. Chem., Int. Ed. **53**, 11629–11633 (2014).

[17]T. Sugimoto, Y. Akahama, H. Fujihisa, Y. Ozawa, H. Fukui, N. Hirao, and Y. Ohishi, "Identification of superlattice structure cI16 in the P-VI phase of phosphorus at 340 GPa and room temperature via x-ray diffraction," Phys. Rev. B **86**, 024109 (2012).

[18]H. Luo, R. G. Greene, and A. L. Ruoff, "β-Po phase of sulfur at 162 GPa: X-Ray diffraction study to 212 GPa," Phys. Rev. Lett. **71**, 2943 (1993).

[19]A. R. Oganov and C. W. Glass, "Crystal structure prediction using *ab initio* evolutionary techniques: Principles and applications," J. Chem. Phys. **124**, 244704 (2006).

[20]T. Rödl, R. Weihrich, J. Wack, J. Senker, and A. Pfitzner, "Rational syntheses and structural characterization of sulfur-rich phosphorus polysulfides: α-P_2S_7 and β-P_2S_7," Angew. Chem., Int. Ed. **50**, 10996–11000 (2011).

[21]Y. C. Leung, J. Waser, S. v. Houten, A. Vos, G. A. Wiegers, and E. H. Wiebenga, "The crystal structure of P_4S_3," Acta Crystallogr. **10**, 574–582 (1957).

[22]B. Wallis, G.-U. Wolf, and P. Leibnitz, "Über die struktur einer neuen modifikation des phosphorsulfids P_4S_9," Z. Anorg. Allg. Chem. **588**, 139–146 (1990).

[23]A. Vos, R. Olthof, F. van Bolhuis, and R. Botterweg, "Refinement of the crystal structures of some phosphorus sulphides," Acta Crystallogr. **19**, 864–867 (1965).

[24]S. Van Houten and E. H. Wiebenga, "The crystal structure of P_4S_5," Acta Crystallogr. **10**, 156–160 (1957).

[25]D. Wei, J. Yin, Z. Ju, S. Zeng, H. Li, W. Zhao, Y. Wei, and H. Li, "Cage-like P_4S_3 molecule as promising anode with high capacity and cycling stability for $Li^+/Na^+/K^+$ storage," J. Energy Chem. **50**, 187–194 (2020).

[26]M. Li, X. Liu, Q. Li, Z. Jin, W. Wang, A. Wang, Y. Huang, and Y. Yang, "P_4S_{10} modified lithium anode for enhanced performance of lithium-sulfur batteries," J. Energy Chem. **41**, 27–33 (2020).

[27]H. Katzke and P. Tolédano, "Displacive mechanisms and order-parameter symmetries for the A7-incommensurate-bcc sequences of high-pressure reconstructive phase transitions in Group Va elements," Phys. Rev. B **77**, 024109 (2008).

[28]A. Shamp, T. Terpstra, T. Bi, Z. Falls, P. Avery, and E. Zurek, "Decomposition products of phosphine under pressure: PH_2 stable and superconducting?," J. Am. Chem. Soc. **138**, 1884–1892 (2016).

[29]J. A. Flores-Livas, M. Amsler, C. Heil, A. Sanna, L. Boeri, G. Profeta, C. Wolverton, S. Goedecker, and E. Gross, "Superconductivity in metastable phases of phosphorus–hydride compounds under high pressure," Phys. Rev. B **93**, 020508 (2016).
[30]H. Liu, Y. Li, G. Gao, J. S. Tse, and I. I. Naumov, "Crystal structure and superconductivity of PH_3 at high pressures," J. Phys. Chem. C **120**, 3458–3461 (2016).
[31]Y. Yuan, Y. Li, G. Fang, G. Liu, C. Pei, X. Li, H. Zheng, K. Yang, and L. Wang, "Stoichiometric evolutions of PH_3 under high pressure: Implication for high-T_c superconducting hydrides," Natl. Sci. Rev. **6**, 524–531 (2019).
[32]A. P. Drozdov, M. I. Eremets, I. A. Troyan, V. Ksenofontov, and S. I. Shylin, "Conventional superconductivity at 203 K at high pressures in the sulfur hydride system," Nature **525**, 73–76 (2015).
[33]Y. Ge, F. Zhang, R. P. Dias, R. J. Hemley, and Y. Yao, "Hole-doped room-temperature superconductivity in $H_3S_{1-x}Z_x$ (Z = C, Si)," Mater. Today Phys. **15**, 100330 (2020).
[34]Y. Ge, F. Zhang, and Y. Yao, "First-principles demonstration of superconductivity at 280 K in hydrogen sulfide with low phosphorus substitution," Phys. Rev. B **93**, 224513 (2016).
[35]F. Fan, D. A. Papaconstantopoulos, M. J. Mehl, and B. M. Klein, "High-temperature superconductivity at high pressures for $H_3Si_xP_{1-x}$, $H_3P_xS_{1-x}$, and $H_3Cl_xS_{1-x}$," J. Phys. Chem. Solids **99**, 105–110 (2016).
[36]M. Amsler, "Thermodynamics and superconductivity of $S_xSe_{1-x}H_3$," Phys. Rev. B **99**, 060102 (2019).
[37]N. Geng, T. Bi, and E. Zurek, "Structural diversity and superconductivity in S–P–H ternary hydrides under pressure," J. Phys. Chem. C **126**, 7208 (2022).
[38]Y. Sun, Y. Tian, B. Jiang, X. Li, H. Li, T. Iitaka, X. Zhong, and Y. Xie, "Computational discovery of a dynamically stable cubic SH_3-like high-temperature superconductor at 100 GPa via CH_4 intercalation," Phys. Rev. B **101**, 174102 (2020).
[39]Z. Shao, D. Duan, Y. Ma, H. Yu, H. Song, H. Xie, D. Li, F. Tian, B. Liu, and T. Cui, "Ternary superconducting cophosphorus hydrides stabilized via lithium," npj Comput. Mater. **5**, 104 (2019).
[40]X. Li, Y. Xie, Y. Sun, P. Huang, H. Liu, C. Chen, and Y. Ma, "Chemically tuning stability and superconductivity of P–H compounds," J. Phys. Chem. Lett. **11**, 935–939 (2020).
[41]X. Li, X. Zhang, A. Bergara, G. Gao, Y. Liu, and G. Yang, "Superconducting LaP_2H_2 with graphene like phosphorus layers," Phys. Rev. B **105**, 024504 (2022).
[42]Y.-L. Li, E. Stavrou, Q. Zhu, S. M. Clarke, Y. Li, and H.-M. Huang, "Superconductivity in the van der Waals layered compound PS_2," Phys. Rev. B **99**, 220503 (2019).
[43]Y. Liu, C. Wang, X. Chen, P. Lv, H. Sun, and D. Duan, "Pressure-induced structures and properties in P–S compounds," Solid State Commun. **293**, 6–10 (2019).
[44]J. P. Perdew, J. A. Chevary, S. H. Vosko, K. A. Jackson, M. R. Pederson, D. J. Singh, and C. Fiolhais, "Atoms, molecules, solids, and surfaces: Applications of the generalized gradient approximation for exchange and correlation," Phys. Rev. B **46**, 6671–6687 (1992).
[45]G. Kresse and J. Furthmüller, "Efficient iterative schemes for *ab initio* total-energy calculations using a plane-wave basis set," Phys. Rev. B **54**, 11169–11186 (1996).
[46]P. E. Blöchl, "Projector augmented-wave method," Phys. Rev. B **50**, 17953–17979 (1994).
[47]A. D. Becke and K. E. Edgecombe, "A simple measure of electron localization in atomic and molecular systems," J. Chem. Phys. **92**, 5397–5403 (1990).
[48]R. Nelson, C. Ertural, J. George, V. L. Deringer, G. Hautier, and R. Dronskowski, "LOBSTER: Local orbital projections, atomic charges, and chemical-bonding analysis from projector-augmented-wave-based density-functional theory," J. Comput. Chem. **41**, 1931–1940 (2020).
[49]A. Togo, F. Oba, and I. Tanaka, "First-principles calculations of the ferroelastic transition between rutile-type and $CaCl_2$-type SiO_2 at high pressures," Phys. Rev. B **78**, 134106 (2008).
[50]P. Giannozzi, S. Baroni, N. Bonini, M. Calandra, R. Car, C. Cavazzoni, D. Ceresoli, G. L. Chiarotti, M. Cococcioni, I. Dabo, A. Dal Corso, S. de Gironcoli, S. Fabris, G. Fratesi, R. Gebauer, U. Gerstmann, C. Gougoussis, A. Kokalj, M. Lazzeri, L. Martin-Samos, N. Marzari, F. Mauri, R. Mazzarello, S. Paolini, A. Pasquarello, L. Paulatto, C. Sbraccia, S. Scandolo, G. Sclauzero, A. P. Seitsonen, A. Smogunov, P. Umari, and R. M. Wentzcovitch, "QUANTUM ESPRESSO: A modular and open-source software project for quantum simulations of materials," J. Phys.: Condens. Matter **21**, 395502 (2009).
[51]O. Degtyareva, E. Gregoryanz, M. Somayazulu, P. Dera, H.-K. Mao, and R. J. Hemley, "Novel chain structures in group VI elements," Nat. Mater. **4**, 152–155 (2005).
[52]J. R. Van Wazer, "Principles of phosphorus chemistry. I. Some generalities concerning multiple bonding," J. Am. Chem. Soc. **78**, 5709–5715 (1956).
[53]T. K. Chattopadhyay, W. May, H. G. von Schnering, and G. S. Pawley, "X-ray and neutron diffraction study of the crystal structure of α-P_4S_3," Z. Kristallogr. - Cryst. Mater. **165**, 47–64 (1983).
[54]P. B. Allen and R. C. Dynes, "Transition temperature of strong-coupled superconductors reanalyzed," Phys. Rev. B **12**, 905–922 (1975).
[55]P. B. Allen and B. Mitrović, "Theory of superconducting T_c," Solid State Phys. **37**, 1–92 (1983).
[56]J. P. Carbotte, "Properties of boson-exchange superconductors," Rev. Mod. Phys. **62**, 1027 (1990).
[57]F. Peng, Y. Sun, C. J. Pickard, R. J. Needs, Q. Wu, and Y. Ma, "Hydrogen clathrate structures in rare earth hydrides at high pressures: Possible route to room-temperature superconductivity," Phys. Rev. Lett. **119**, 107001 (2017).
[58]D. V. Semenok, A. G. Kvashnin, A. G. Ivanova, V. Svitlyk, V. Y. Fominski, A. V. Sadakov, O. A. Sobolevskiy, V. M. Pudalov, I. A. Troyan, and A. R. Oganov, "Superconductivity at 161 K in thorium hydride ThH_{10}: Synthesis and properties," Mater. Today **33**, 36–44 (2020).
[59]D. Zhou, D. V. Semenok, D. Duan, H. Xie, W. Chen, X. Huang, X. Li, B. Liu, A. R. Oganov, and T. Cui, "Superconducting praseodymium superhydrides," Sci. Adv. **6**, eaax6849 (2020).
[60]A. Nakanishi, T. Ishikawa, and K. Shimizu, "First-principles study on superconductivity of P- and Cl-doped H_3S," J. Phys. Soc. Jpn. **87**, 124711 (2018).
[61]T. Wang, M. Hirayama, T. Nomoto, T. Koretsune, R. Arita, and J. A. Flores-Livas, "Absence of conventional room-temperature superconductivity at high pressure in carbon-doped H_3S," Phys. Rev. B **104**, 064510 (2021).
[62]Y. Li, L. Wang, H. Liu, Y. Zhang, J. Hao, C. J. Pickard, J. R. Nelson, R. J. Needs, W. Li, and Y. Huang, "Dissociation products and structures of solid H_2S at strong compression," Phys. Rev. B **93**, 020103 (2016).
[63]P. Morel and P. W. Anderson, "Calculation of the superconducting state parameters with retarded electron-phonon interaction," Phys. Rev. **125**, 1263–1271 (1962).
[64]A. Sanna, J. A. Flores-Livas, A. Davydov, G. Profeta, K. Dewhurst, S. Sharma, and E. K. U. Gross, "*Ab initio* Eliashberg theory: Making genuine predictions of superconducting features," J. Phys. Soc. Jpn. **87**, 041012 (2018).